

# Studying High Redshift Star Forming Galaxies at Centimeter and Millimeter Wavelengths

C. L. Carilli<sup>1,2</sup>, K. M. Menten<sup>2</sup>, M. S. Yun<sup>1</sup>, F. Bertoldi<sup>2</sup>, F. Owen<sup>1</sup>, A. Dey<sup>3</sup>

<sup>1</sup>National Radio Astronomy Observatory, Socorro, NM, USA, ccarilli@nrao.edu

<sup>2</sup>Max-Planck-Institut für Radioastronomie, Bonn, Germany

<sup>3</sup>National Optical Astronomy Observatory, Tucson, AZ, USA

We discuss various aspects of centimeter and millimeter wavelength continuum and line observations of high redshift star forming galaxies. Perhaps the most important lesson is that sensitive observations at submm through cm wavelengths reveal a population of active star forming galaxies at high redshift which are unseen in deep optical surveys due to dust obscuration. Current models suggest that this population represents the formation of the spheroidal components of galaxies at  $z$  between 2 and 5, constituting about half of the total amount of cosmic star formation from the big bang to the present. High resolution imaging at cm wavelengths provides sub-arcsecond astrometry, and can be used to search for gravitational lensing and/or for the presence of an AGN. Radio continuum observations provide unique information on the magnetic fields in early galaxies, and give a gross indication of the star formation rate, while the radio-to-submm spectral index provides a rough indication of source redshift. Low  $J$  transitions of CO are redshifted into the cm bands for  $z > 2$ , allowing for sensitive searches for CO emission over large volumes at high redshift. We present recent results from the Very Large Array (VLA), and from the new 230 GHz MPIFR bolometer array at the IRAM 30m telescope. A wide field survey with the bolometer array indicates a cut-off in the source distribution function at FIR luminosities  $> 3 \times 10^{12} L_{\odot}$ . Lastly, we summarize the scientific promise of the New VLA.

To appear in *Scientific Imperatives at centimeter and meter Wavelengths*, ed. M.P van Haarlem and J.M. van der Hulst, (Dwingeloo: NFRA).

## 1 Introduction

The sharp rise of observed flux density,  $S_{\nu}$ , with increasing frequency,  $\nu$ , in the Rayleigh-Jeans portion of the grey-body spectrum for thermal dust emission from star forming galaxies ( $S_{\nu} \propto \nu^{3.25}$ ), leads to a dramatic negative  $K$ -correction for observed flux density with increasing redshift. Submm surveys thereby provide a uniquely *distance independent* sample of objects in the universe, meaning the observed submm flux density of an object of given intrinsic luminosity is roughly constant, or even increases substantially for certain cosmologies, for  $z$  between 1 and 5 for a fixed observing frequency (Blain & Longair 1993).

Initial studies of optical galaxies in the Hubble Deep Field suggested a sharp peak in the cosmic star formation density at around  $z = 1.5$  (Madau et al. 1996). However, recent observations of faint submm source counts argue that the cosmic star formation rate may be roughly constant between  $z = 1$  to 5, implying that optical studies may be missing a substantial amount of star formation occurring in dust-obscured starbursts at high  $z$  (Hughes et al. 1998, Eales et al. 1999, Blain et al. 1999a). This notion appears to have been confirmed through new optical observations of high  $z$  galaxies by including larger dust-extinction corrections (Steidel et al. 1999, Calzetti & Heckman 1999).

Tan, Silk, & Blanford (1999) have presented a model of the star formation history of the universe which may explain the faint source counts from the optical through the radio regimes. They hypothesize that star formation occurs in two phases. At high redshift ( $2 < z < 5$ ), very active star formation, with rates  $\geq 100 M_{\odot} \text{ year}^{-1}$ , occurs in merger events leading to the

formation of the spheroidal components of galaxies (spiral bulges and ellipticals; Barger, Cowie, & Sanders 1999). At lower redshift ( $z < 2$ ), the stellar disks of galaxies are formed over longer periods at lower star formation rates. The high  $z$  starbursts are dusty systems and are revealed primarily as constituents of the faint submm, IR, and radio source populations. In contrast, the faint optical source counts are dominated by the lower  $z$  disk-forming systems. Tan et al. state that the early spheroids may act as “seeds” for disk formation as gas falls in, and that the present-day stellar mass in bulges and halos is comparable to that in disks, i.e. that about half of the total amount of the star formation in the universe has occurred in these dusty, high  $z$  starbursts. Moreover, this population of high  $z$  star-forming galaxies may provide a significant contribution to cosmic metal production (Fall & Pei 1999), and to the re-ionization of the universe at  $z > 3$  (Baltz, Gnedin, & Silk 1998).

Given the tight radio-to-far infrared (FIR) correlation in star-forming galaxies (Condon 1992), the mJy submm source population can be equated with, for the most part, the  $\mu$ Jy radio source population. Observations at cm wavelengths can provide important information on high  $z$  star-forming galaxies, complementary to mm, submm, and near IR observations:

- Radio interferometry offers sub-arcsecond astrometry, which is critical for faint source identification in confused optical and near IR fields (Blain 1999, Smail et al. 1999).
- The submm-to-cm spectral index provides a rough indication of source redshift (Carilli & Yun 1999, Blain 1999). The redshift distribution of the faint submm source population is a key parameter for constraining models of the star formation history of the universe using submm source counts, and presently a point of serious debate (Blain et al. 1999b).
- High resolution radio imaging provides information on a number of issues, including: (i) the existence of an active nucleus, (ii) the distribution of star formation in early galaxies, and (iii) the possibility of gravitational lensing.
- Radio continuum emission contains unique information on the strength and structure of magnetic fields in early galaxies (Beck et al. 1996).
- Radio continuum emission provides an indication of the star formation rate, via the tight radio-to-FIR correlation for star forming galaxies (Condon 1992).
- CO emission involving low rotational quantum numbers ( $J$ ) are redshifted to cm wavelengths for  $z \geq 2$ .

In this contribution we discuss various aspects of continuum and line observations of high redshift star forming galaxies at cm wavelengths. We present recent results from the Very Large Array, and discuss the future capabilities after the VLA expansion (the ‘New VLA’). We assume  $H_0 = 75 \text{ km s}^{-1} \text{ Mpc}^{-1}$  and  $q_0 = 0.5$ .

## 2 The Radio-to-FIR Spectral Index as a Redshift Indicator

The most difficult aspect of studying star forming galaxies at high redshift is determining the redshift. Redshifts are critical for constraining models of the star formation history of the universe using faint submm source counts. However, the study of the faint submm source population shows that the more active star forming galaxies at high redshift are highly dust-obscured, and hence challenging to study even with the largest optical telescopes, with typical magnitudes of  $I > 25$ , and colors  $I - K \geq 4$  (Smail et al. 1999, Cimatti et al. 1998).

We have recently considered the possibility of using the radio-to-FIR spectral index as a gross indicator of redshift for star forming galaxies (Carilli & Yun 1999). Blain (1999) has subsequently re-cast this relationship into a format involving the logarithm of flux density ratio. The spectral index is related to the logarithm of the flux density ratio simply by a factor  $2.4 = \log\left[\frac{350}{1.4}\right]$ . The technique is based on the very tight correlation found between the radio

and far IR emission from star forming galaxies, and the effect is demonstrated in Figure 1. The 1.4 GHz to 350 GHz spectral index will change from about 0 at low redshift, to about 1 at  $z > 3$  for a star forming galaxy with an SED similar to M82. This is not a subtle effect – a unit change in the spectral index corresponds to a change in flux density ratio by a factor 250. We emphasize that there is significant scatter in the observed value for galaxies at a given redshift, such that this technique should be used simply as a redshift ‘indicator’ (i.e. low  $z$  versus high  $z$ ), analogous to the optical ‘drop-out’ technique, and not as a redshift ‘estimator’. Still, even a gross indication of the source redshift distribution is an important model constraint (Smail et al. 1999).

Carilli & Yun (1999) and Blain (1999) discuss the origin of the scatter in the relationship. Two possibly important effects in the radio are free-free absorption at low frequency, and inverse Compton losses off the microwave background at high redshift, while in the submm the dust temperature can alter the relationship substantially. The models in Figure 1 are for a dust temperature of about 50 K, as is found in the starburst nucleus of M82 (Güsten et al. 1993). Temperatures around this value appear to be prevalent for high  $z$  starburst systems (Benford et al. 1999). Of course, the presence of a radio loud AGN will invalidate the relationship. Turning this around, given a source redshift, this relationship can be used to test for the existence of a radio loud AGN. As examples, the presence of a radio loud AGN can be seen for the two sources 1413+117 and 0952–0115 in Figure 1. Contamination of submm samples by radio loud AGN is thought to be  $\leq 10\%$  (Yun, Reddy, & Condon in preparation).

### 3 The Hubble Deep Field

The Hubble Deep Field (HDF) has played a dominant role in the study of galaxy evolution over the last few years. Deep optical imaging has revealed thousands of galaxies in a region of only a few square minutes. At first glance, radio and submm observations of the HDF appear to be disappointing – with only a handful of firm detections at 1.4 GHz (Richards et al. 1999), and even fewer at 350 GHz (Hughes et al. 1998). There are many simulations in this volume which demonstrate how the SKA will detect most of the galaxies in the HDF with reasonable integration times.

However, we would like to emphasize that the existing cm and submm data on the HDF already have a profound consequence: thus far there is no convincing optical identification of the brightest submm source in the HDF (Downes et al. 1999). Based on deep imaging at 230 GHz using the Plateau de Bure interferometer, and VLA imaging at 1.4 GHz, the submm and radio source is situated between an elliptical galaxy at  $z = 1.12$  and a faint arc of emission with an unknown redshift (Downes et al. 1999, Figure 2). The source is 7 mJy at 350 GHz (Hughes et al. 1998), and 15  $\mu$ Jy at 1.4 GHz (Richards et al. 1999), implying  $z > 3$  based on the relationship shown in Figure 1.

This observation of the HDF is a dramatic demonstration that the mJy submm and  $\mu$ Jy radio source counts reveal a population of sources that are essentially unseen in the deepest optical observations. Until the advent of the NGST, systematic study of a large sample of these sources will be the exclusive regime of radio through infrared observations (Blain 1999), with optical follow-up observations limited to a few objects using long integrations on the largest optical telescopes. It also emphasizes the extreme difficulty and care that must be taken when making optical identifications of faint submm sources based on low spatial resolution data. Deep radio imaging with sub-arcsecond astrometry is critical to any optical follow-up program to study dust obscured, high redshift star forming galaxies.

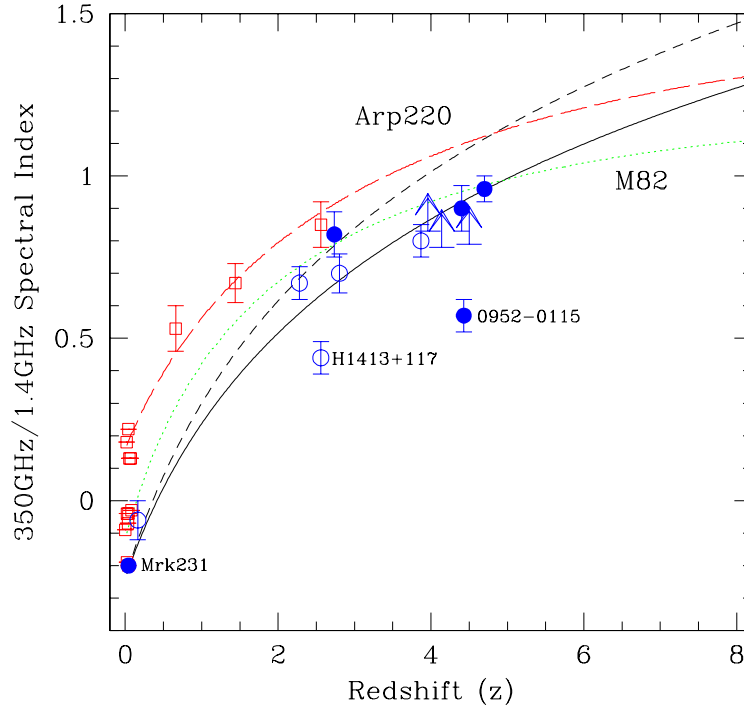
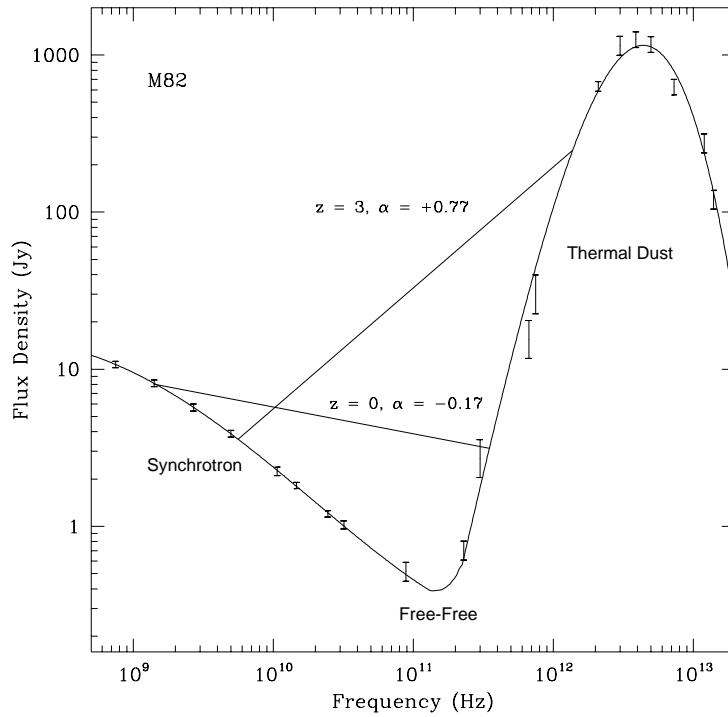


Figure 1: The upper panel shows the radio-thru-infrared SED of M82. The two straight lines show the change in observed spectral index between 1.4 GHz and 350 GHz for a source at  $z = 0$  and  $z = 3$ . The lower panel shows the behavior of the observed 1.4 GHz-to-350 GHz spectral index as a function of source redshift for star forming galaxies. The models are semi-analytic, based on equations in Condon (1992), and empirical models based on observations of Arp 220 and M82. The data points show the results for high redshift submm sources (see Carilli & Yun 1999, and Yun et al. 1999 for details). Note that the position of 1413+117 and 0952-0115 on this diagram indicate the existence of a radio-loud AGN.

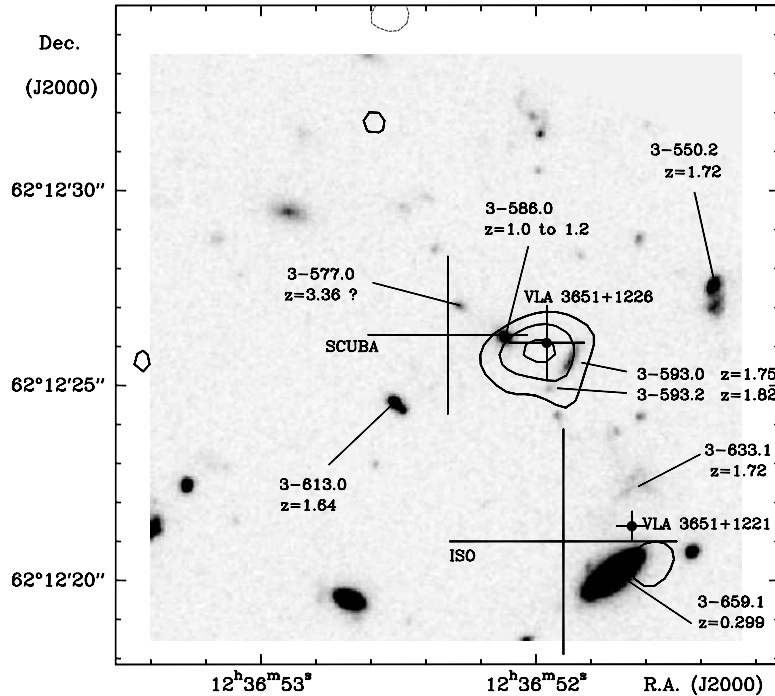


Figure 2: The contours show the 230 GHz continuum emission from HDF 850.1 as observed with the IRAM interferometer (Downes et al. 1999). The grey scale is the HST image of the field. A cross marks the position of the radio continuum source. The redshifts indicated are very tentative, as derived in Downes et al. (1999) from marginal optical broad band photometry. These require confirmation. Radio and submm data suggest a large redshift for the 230 GHz source ( $z \geq 3$ ).

#### 4 Star Formation and Massive Black Holes at High Redshift

Omont et al. (1996) have made the remarkable discovery that a significant fraction of optically selected high  $z$  QSOs show thermal dust emission. Of their sample of 16 QSOs at  $z > 4$ , a total of 6 sources show dust emission at 230 GHz, with implied dust masses of  $10^8$  to  $10^9 M_{\odot}$ . Follow-up mm line observations of three of these dust emitting QSOs have revealed CO emission with implied molecular gas masses  $\sim 10^{11} M_{\odot}$  (Ohta et al. 1996; Guilloteau et al. 1997). Omont et al. (1996) speculate that “. . . such large amounts of dust [and gas] imply giant starbursts at  $z > 4$ , at least comparable to those found in the most hyper-luminous IRAS galaxies. . .”. However, the evidence for active star formation in these sources remains circumstantial, primarily based on the presence of large gas reservoirs. It remains possible that the dust is heated by the active galactic nucleus (AGN), rather than by a starburst.

We have used the VLA to study the radio continuum and CO(2–1) emission from one of these systems, 1335–0417, at  $z = 4.4$ . The CO(2–1) line redshifts into the 43 GHz band of the VLA for  $4.9 > z > 3.8$  (Figure 3). We have detected CO emission at 43 GHz, and radio continuum emission at 1.4 and 5 GHz, from 1335–0417 using the VLA (Carilli, Menten, & Yun 1999). We find that the ratio of the velocity-integrated line intensity for the CO(2–1) and CO(5–4) emission (Guilloteau et al. 1997) from 1335–0417 is consistent with constant brightness temperature (i.e. integrated line flux increasing as  $\nu^2$ ), implying optically thick emission in both lines, for a fixed source size. Constant brightness temperature implies that the molecular gas must be fairly warm, with a lower limit to the rotational temperature of 30 K set by the excitation of the CO (5–4) line, and that the line emission is optically thick. A lower limit to the source size can be derived assuming a single, homogeneous, optically thick emitting region (Ohta et al. 1996). The beam filling factor is given by:  $\frac{\Omega_s}{\Omega_b} = \frac{T_{\text{obs}}}{T_{\text{ex}}} \times (1 + z)$ , where  $\Omega_s$  and  $\Omega_b$  are the source and beam solid angles, respectively,  $T_{\text{obs}}$  is the observed line brightness temperature, and the line excitation temperature,  $T_{\text{ex}}$ , is assumed to be equal to the intrinsic

(rest frame) source brightness temperature. Note that for a resolved source, the observed brightness temperature obeys:  $T_{\text{obs}} = \frac{T_{\text{ex}}}{(1+z)}$ . We find that the minimum source diameter for 1335–0417 is  $0''.23 \times (\frac{T_{\text{ex}}}{50\text{K}})^{-\frac{1}{2}}$ .

The critical question concerning 1335–0417 is whether the dust and radio continuum emission are powered by the AGN, or star formation, or both. Figure 3 shows the integrated spectral energy distribution for 1335–0417 for rest frame frequencies from 7.6 GHz up to 4600 GHz, normalized to the spectrum of the nuclear starburst galaxy M82. For demonstrative purposes we have quantified the spectrum of M82 using two accurate polynomial fits: one to the synchrotron emission which dominates at frequencies below 100 GHz, and a second to the thermal dust emission which dominates above 100 GHz. All the data points for 1335–0417 fall within  $2\sigma$  of the M82 curve. The agreement between the SED of 1335–0417 with that of M82 argues in favor of star formation playing the dominant role in heating the dust and powering the radio continuum emission from 1335–0417. It is important to note that, while the shapes of the SEDs are similar, the luminosity of 1335–0417 is  $1.2 \times 10^{32}$  ergs  $\text{s}^{-1}$   $\text{Hz}^{-1}$  at 1.47 GHz in the rest frame of the source, assuming a radio spectral index of  $-0.8$ , while that of M82 is a factor 1400 lower (assuming a distance of 3 Mpc to M82). If the emission is powered by star formation, a very rough estimate of the massive star formation rate in 1335–0417 can be derived from the radio and submm continuum emission using equations 1 and 2 in Carilli & Yun (1999). Both values are consistent with a massive star formation rate of  $2300 \pm 600 M_{\odot} \text{yr}^{-1}$ . We emphasize that this is at best an order-of-magnitude estimate.

Overall, the cm and mm continuum observations, as well as the CO line data, argue in favor of a very massive starburst concurrent with the AGN activity in 1335–0417 at  $z = 4.4074$ . A similar conclusion has been reached concerning a number of other dust emitting QSOs from the Omont et al. sample by Yun et al. (1999). The gas depletion timescale is short,  $\leq 10^9$  years, in which time a significant fraction of the stars in the host galaxy of the AGN may be formed (Benford et al. 1999).

## 5 Bright Faint Source Survey

A major new instrument in the study of faint mm sources is the MPIfR 230 GHz, 37 element bolometer camera on the IRAM 30m telescope (Kreysa et al. 1999). The sensitivity of this instrument, coupled with the better atmosphere at 230 GHz relative to 350 GHz, and the large aperture of the 30m telescope makes this instrument competitive with SCUBA on the JCMT at 350 GHz (Holland et al. 1999), even including the sharply rising spectrum of thermal sources. We had a long observing session using this camera on the 30m during February and March, 1999. The initial results indicate that an rms sensitivity of 0.4 mJy can be reached in 5 hours under good conditions for on-off observations of point sources.

One of the initial observing programs was wide field imaging of the field around the  $z = 0.27$  cluster A2125. We chose this field because very deep radio imaging has been performed at the VLA, to a sensitivity level of  $6\mu\text{Jy}$  at 1.4 GHz (Owen & Morrison, in prep.). The existence of a cluster may help to enhance the faint source counts through gravitational lensing (Blain et al. 1999), at least within a few arcmin of the cluster center. It was decided to image a relatively large field to a moderate sensitivity level, in order to study the high-end of the source luminosity function (the ‘Bright-Faint’ sources). Also, it can be shown that as long as the index for the source luminosity function is less than 2, this type of medium sensitivity, wide-field mapping procedure is the most efficient in terms of maximizing the number of sources detected with a given total observing time. Detecting a large number of sources over a wide field will allow us to study source clustering properties on scales from 100 kpc to 2 Mpc, in order to test the current idea that the faint submm sources may be the precursors of present day elliptical galaxies (Smail et al. 1999, Tan et al. 1999).

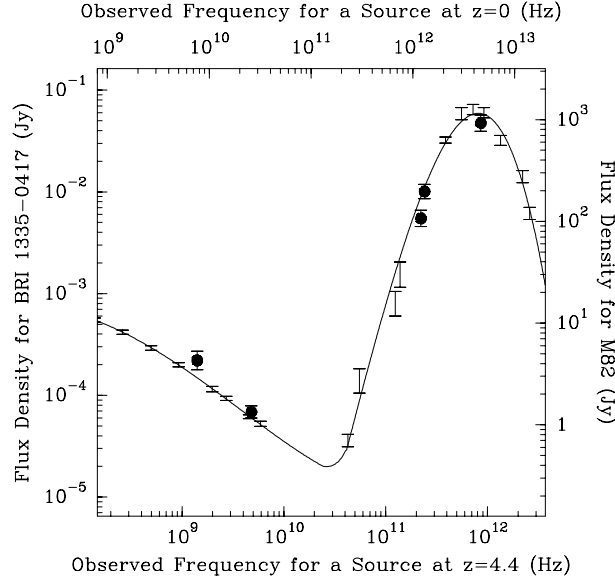
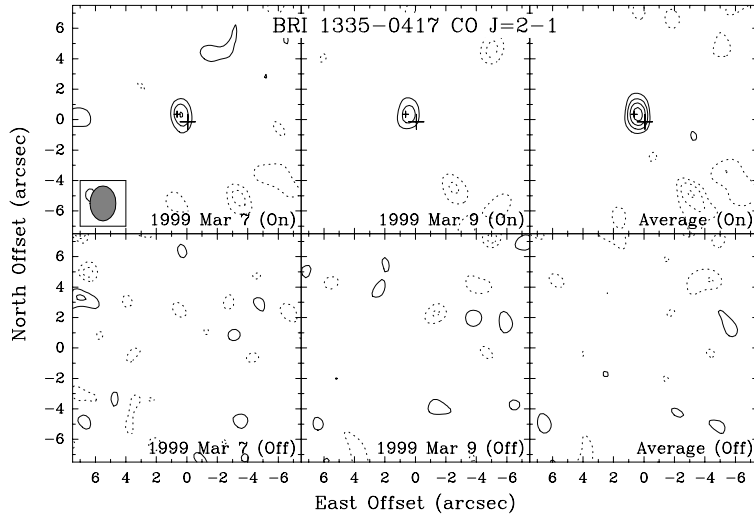


Figure 3: The upper panel shows VLA contour maps of 1335–0417 taken at a frequency centered on (upper panels), and off (lower panels) the frequency of the redshifted ( $z = 4.4074$ ) CO (2–1) line emission near 43 GHz. The leftmost and middle panels show the maps produced from data taken on 1999 March 7 and 9, respectively, while the rightmost map was produced from the average of these individual datasets. The contour levels represent  $-4$ ,  $-3$ ,  $-2$ ,  $2$ ,  $3$ ,  $4$ , and  $5$  times the  $1\sigma$  rms noise, which is  $0.19 \text{ mJy beam}^{-1}$  for the “single day” maps and  $0.13 \text{ mJy beam}^{-1}$  for the map made from the averaged data. The maps have been restored with a beam of size  $2''.3 \times 1''.7$  (FWHM) elongated N-S, which is indicated by the grey ellipse in the leftmost “on” map. The small cross marks the position of the 1.35 mm dust continuum source determined by Guilloteau et al. 1997, with the size of the cross indicating the  $\pm 0''.2$  uncertainty of the mm position. The larger cross marks the optical position given by Storrie-Lombardi et al. 1996 without errors quoted. In the lower panel, the solid line shows the radio through infrared spectral energy distribution (SED) of M82 derived via polynomial fits to the observed data points, which are taken from the NASA Extragalactic Data Base (NED) and are shown as vertical error bars. The solid dots (plus error bars) show the data for the  $z = 4.4074$  QSO 1335–0417. For comparative purposes, the data for 1335–0417 have been normalized to the SED of M82 using the mean of the normalization value at rest frame frequencies of 26 GHz and 1300 GHz. The left and right hand flux density scales are those appropriate for 1335–0417 and M82, respectively. Note that the intrinsic luminosity at 1.4 GHz of 1335–0417 is a factor 1400 times larger than that of M82. The lower abscissa is chosen to represent the observed frequency scale for the 1335–0417 data points (i.e. for a source at  $z = 4.4$ ), whereas the upper abscissa is appropriate for the M82 data points (i.e. for a source at  $z = 0$ ).

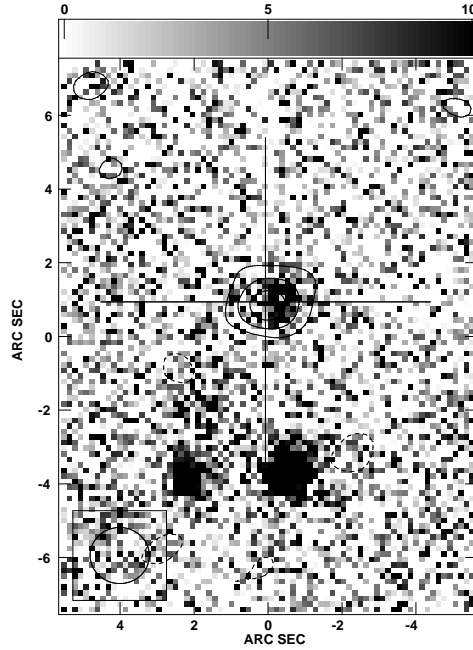


Figure 4: The contours show the 1.4 GHz emission from a  $70\mu\text{Jy}$  source in the A2125 field, with levels -36, -18, 18, 36, 54, and  $72\mu\text{Jy}/\text{beam}$ . The grey scale is a K band image of the field from the Keck telescope. The cross marks the position of a 3 mJy source at 230 GHz, and the cross size is the FWHM of the IRAM 30m primary beam.

Smail et al. (1999) present a cumulative source distribution that is consistent with a power-law of the form:  $N(> S) = 1800 \times (S_{230})^{-1.1} \text{ deg}^{-2}$ , where  $S_{230}$  is the flux density in mJy at 230 GHz (Smail et al. 1999), assuming a submm spectral index of +3.25, leading to a factor 4 lower flux density at 230 GHz relative to 350 GHz. Barger, Cowie, & Richards (1999) obtain a somewhat steeper distribution, with a possible cut-off at  $S_{230} \geq 2$  mJy, although the statistics at high flux levels remain limited. To date, we have surveyed a total area of about  $100 \text{ arcmin}^2$  to an rms sensitivity of  $\leq 1$  mJy at 230 GHz with the MPI bolometer array at the IRAM 30m. Using the Smail et al. (1999) source distribution, we would expect to detect about 25 sources above 2 mJy, and 14 sources above 3.5 mJy. We find about 10 sources between 2 and 3.5 mJy, and no sources above 3.5 mJy. This is consistent with the possible cut-off at high luminosities suggested by Barger et al. (1999). Note that 2 mJy at 230 GHz corresponds to an FIR luminosity of about  $3 \times 10^{12} L_{\odot}$ , or a massive star formation rate of about  $470 M_{\odot} \text{ year}^{-1}$  (Cowie & Barger 1999, Carilli & Yun 1999).

Figure 4 shows one of the sources we have detected in the A2125 field. The source is 3 mJy at 230 GHz. It is coincident with a  $70\mu\text{Jy}$  radio source. Nothing is seen at the position in the optical to  $R > 24.5$ . A deep K band image taken with the Keck telescope reveals a source at the expected position with  $K = 21$ . Based on the radio-to-submm spectral index, this source is likely to be at  $z > 2$ . Note that within the  $12''$  (FWHM) beam of the 30m telescope there are three faint near IR sources. The radio continuum emission provides an unambiguous identification of the 230 GHz source. Again, these observations are meant to illustrate the importance of deep radio imaging with sub-arcsecond resolution for accurate source identification, and the difficulty of follow-up optical identification for these very faint, red sources (Cimatti et al. 1998).



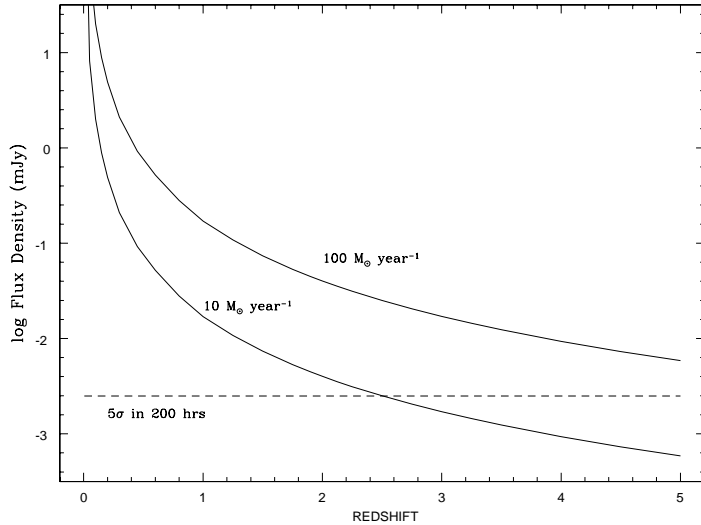


Figure 5: The expected radio continuum flux density at 1.4 GHz of star forming galaxies as a function of redshift. The flux densities were derived using the relationships in Condon (1992). The dashed line shows the  $5\sigma$  sensitivity of the New VLA in 200 hrs.

## 6 Near Future: The New VLA

The science case for studying high redshift star forming galaxies with the Atacama Large Millimeter Array (ALMA), is well documented (see MMA home page on <http://www.nrao.edu>), while that for the SKA is spelled-out in detail in this volume. In this section we discuss the nearer-term possibilities that will arise with the expanded VLA within the next 5 years. A good discussion of the synergy between the submm, mm, and cm observations with future instrumentation can be found in Blain (1999).

The principal aspect of the VLA expansion is a wideband ( $4 \times 2$  GHz  $\times$  2 polarizations) correlator with greatly increased spectral capabilities. The expansion also includes: (i) upgrades to existing receivers to decrease system noise and to provide complete frequency coverage from 1.0 to 50 GHz, (ii) improvements to antenna pointing and efficiency, and, on a longer timescale, (iii) additional antennas extending the maximum baseline by a factor of 10 to 300 km (see VLA upgrade homepage on <http://www.nrao.edu>). Overall, the VLA expansion represents an improvement by an order of magnitude, or more, for all aspects of observing with the VLA. The New VLA propels cm continuum observation into the realm of sub- $\mu$ Jy sensitivity, while the new spectral line capabilities allow for large volume searches for high redshift CO emission.

Figure 5 shows the expected sensitivity of the New VLA at 1.4 GHz for a long, but not unreasonable integration time (200 hr), as compared with the expected flux density for synchrotron emission from typical star forming galaxies. The New VLA will be able to detect synchrotron emission from massive star forming galaxies ( $100 M_{\odot} \text{ yr}^{-1}$ ) to  $z \sim 5$ , corresponding to sources with 350 GHz flux densities of 2 mJy, and lower star formation rate galaxies ( $10 M_{\odot} \text{ yr}^{-1}$ ) to  $z = 2.5$ . The relationship between massive star formation rate and radio continuum luminosity is taken from Condon (1992). Note that on this scale a typical ultra-luminous infrared galaxy (ULIRG), like Arp 220, has a massive star formation rate  $\approx 100 M_{\odot} \text{ yr}^{-1}$ .

A second important use of the New VLA will be to image low- $J$  CO emission from high redshift galaxies. Figure 6 shows the sensitivity and redshift range covered by the New VLA for the CO(1–0), CO(2–1), and CO(3–2) transitions. We have assumed constant brightness temperature for the lines. We use the expression relating gas mass to CO luminosity from

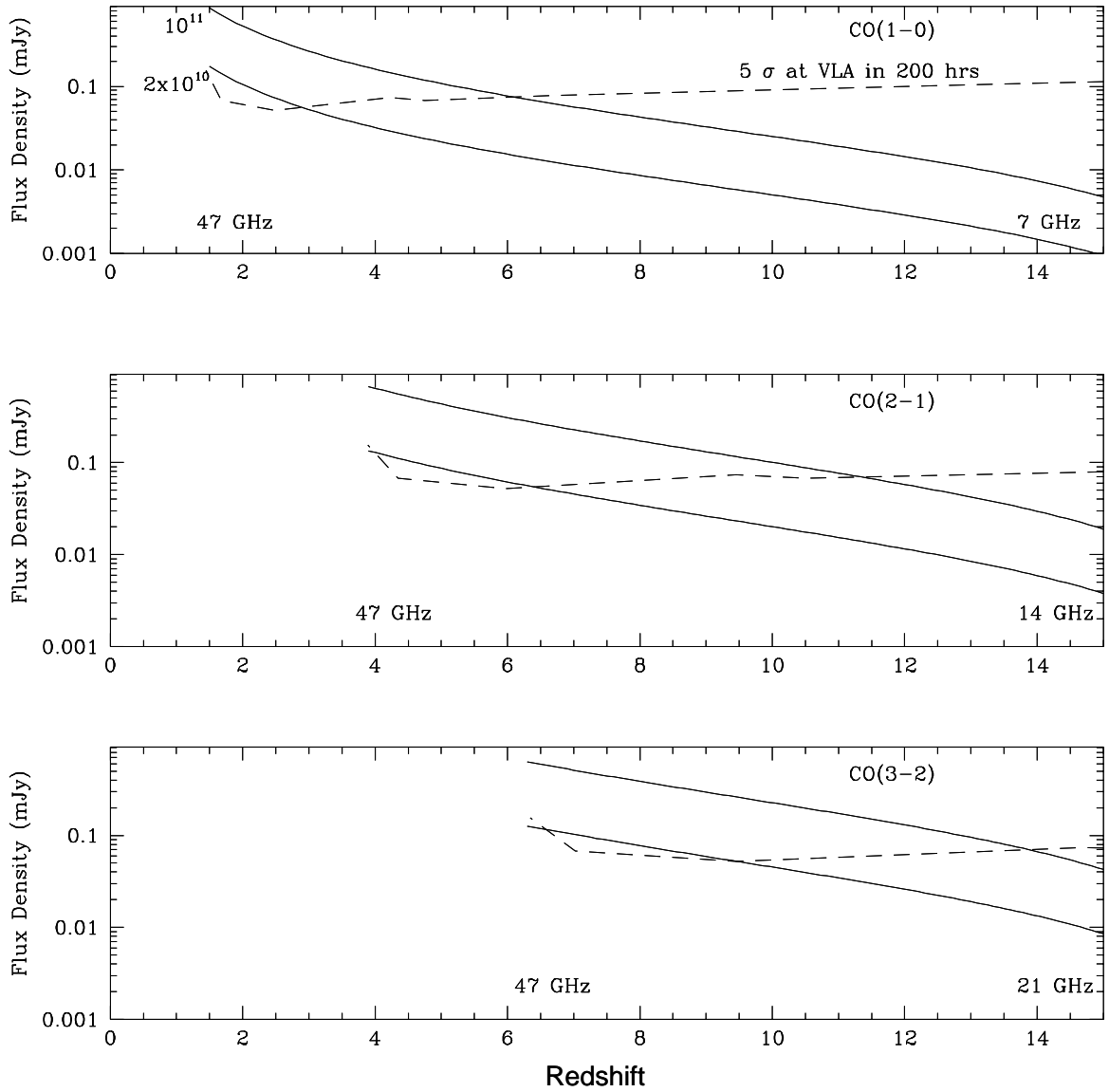


Figure 6: The expected CO emission as a function of redshift for three CO transitions. The upper solid line in each panel is for a molecular gas mass of  $10^{11} M_{\odot}$ , and the lower solid line is for  $2 \times 10^{10} M_{\odot}$ . The flux densities as a function of mass and redshift were derived as described in section 6. In terms of CO luminosity, the ULIRGs Arp 220 and Mrk 231 would both have gas masses of about  $2 \times 10^{10} M_{\odot}$  on the scale in Figure 6, corresponding to the lower solid line in each panel. The dashed line shows the New VLA sensitivity ( $5\sigma$  in 200hrs at  $400 \text{ km s}^{-1}$  resolution). The observing frequency at each end of the curve for a given transition and redshift is listed along the bottom of each panel.

Solomon, Radford, & Downes (1992), with the added factor of line ‘suppression’ due to the microwave background radiation.<sup>a</sup> We adopt a gas temperature of 50 K (Benford et al. 1999). Note that the Solomon et al. expression is derived assuming a Galactic gas mass-to-CO luminosity conversion factor. Current observations suggest that this conversion factor overestimates the gas mass for extreme starburst systems by at least a factor 3 (Carilli et al. 1999, Solomon and Downes 1998). In terms of CO luminosity, the ULIRGs Arp 220 and Mrk 231 would both have gas masses of about  $2 \times 10^{10} M_{\odot}$  on the scale in Figure 6.

The New VLA will be able to detect CO emission from ULIRGs, such as Arp 220, to large redshifts. Moreover, the New VLA will have enough sensitivity and resolution to produce spatially resolved images of the CO emission from these high redshift systems. The New VLA will have a  $1\sigma$  brightness temperature sensitivity in 200 hrs in the B array at 43 GHz of 0.25 K at 200 mas resolution for a line with FWHM = 400 km s<sup>-1</sup>, adequate to image the CO emission from the  $z = 4.4$  QSO 1335–0417 (see section 4). We should also point out that, due to correlator limitations, the current CO observations of 1335–0417 with the VLA were done in continuum mode, using just two channels, an ‘on-line’ and an ‘off-line’ channel each with the maximum bandwidth of 50 MHz, or 350 km s<sup>-1</sup>. The upgraded VLA correlator will provide adequate bandwidth and spectral channels to obtain a proper spectrum of the emission from 1335–0417.

Notice that the expected flux densities for the three CO transitions are roughly the same at any given frequency. For instance, at 30 GHz the three CO transitions, CO(1–0), (2–1), and (3–2), are seen at  $z = 2.8, 6.7,$  and  $10.5,$  respectively, and have expected flux densities of  $27 \mu\text{Jy}, 26 \mu\text{Jy},$  and  $20 \mu\text{Jy},$  respectively for  $10^{10} M_{\odot}$  of gas. This is due to the (reasonable) assumption of constant line brightness temperature. This leads to the interesting capability that any survey for high  $z$  CO emission in these frequency ranges automatically covers a number of redshift ranges at a fairly uniform mass sensitivity limit. As an example, with the New VLA one can envision a search for CO emission using a single frequency setting covering the range of 26 to 34 GHz. The primary beam has FWHM =  $1.4'$ , and the  $5\sigma$  sensitivity at 400 km s<sup>-1</sup> resolution in 200 hrs is about  $70 \mu\text{Jy}.$  This corresponds to the expected CO emission from Arp 220, or about  $2 \times 10^{10} M_{\odot}$  of H<sub>2</sub> using the standard Galactic conversion factor. The redshift ranges, sensitivities, mass limits, comoving volumes, and expected number of sources, are listed in Table 1. The expected number of sources is derived using a comoving density of  $10^{-3} \text{ Mpc}^{-3}$  for high  $z$  sources with 350 GHz flux densities  $\geq 1 \text{ mJy},$  ie. sources with luminosities comparable to, or greater than, that of Arp 220 (Smail et al. 1999, Carilli and Yun 1999b).

Models of cosmic structure formation predict a cosmic ‘dark age’, just prior to the first formation of stars in the universe, sometime between  $z = 6$  and  $15$  (see Rees & Meiksin, this volume). The New VLA will probe the limits of this dark age, revealing radio continuum and molecular line emission from the first generation of star forming galaxies in the universe.

Table 1: A search for redshifted CO emission using the New VLA at 26 to 34 GHz.

Transition	Redshift	Mass limit ( $5\sigma$ ) $\times 10^{10} M_{\odot}$	Comoving Volume $\text{Mpc}^3$	Number of sources
CO(1–0)	2.3 - 3.4	2.4	1300	1.3
CO(2–1)	5.8 - 7.8	2.4	1400	1.4
CO(3–2)	9.0 - 12	3.3	1450	1.4

<sup>a</sup>The line brightness temperature is measured only relative to the background, such that the observed line flux density,  $S_{\text{obs}},$  is decreased relative to the ‘true’ line flux,  $S_{\text{true}}$  (i.e. in the absence of the microwave background radiation), by the factor:  $S_{\text{obs}} = S_{\text{true}} \times (1 - \frac{T_{\text{bg}}}{T_{\text{ex}}}),$  where  $T_{\text{bg}} = 2.73 \times (1 + z).$  In other words, the background radiation is ‘blocked’ by the source.

## Acknowledgements

C.C. acknowledges support from the Alexander von Humboldt society. The National Radio Astronomy Observatory is a facility of Associated Universities, Inc., operated by the National Science Foundation.

## References

- Baltz, E., Gnedin, N., & Silk, J. 1998, *ApJ* (letters), 493, 1
- Barger, A., Cowie, L., & Sanders, D. 1999, *ApJ* (letters), 518, 5
- Barger, A., Cowie, L., & Richards, E. 1999, *astro-ph*. 9907022
- Beck, R., Brandenburg, A., Moss, D. Shukirov, A., & Sokoloff, D. 1996, *ARAA*, 34, 155
- Benford, D. J., Cox, P., Omont, A., Phillips, T. G., & McMahon, R. G. 1999, preprint (*astro-ph/9904277*)
- Blain, A.W. 1999, *astro-ph* 9905248
- Blain, A.W., Kneib, J.P., Ivison, R.J., & Smail, I. 1999, *ApJ* (letters), 512, 87
- Blain, A.W., Smail, I., Ivison, R., & Kneib, J.P. 1999, *MNRAS*, 302, 632
- Blain, A.W., & Longair, M.S. 1993, *MNRAS*, 264, 509
- Calzetti, D. and Heckman, T. *ApJ*, in press, *astro-ph* 9811099
- Carilli, C. L. & Yun, M. S. 1999, *ApJ*, 513, L13
- Carilli, C.L. & Yun, M.S. 1999, *ApJ*, submitted
- Carilli, C.L., Menten, K.M., & Yun, M.S. 1999, *ApJ* (letters), 521, 25
- Cimatti, A., &reani, P., Rottgering, H., & Tilanus, R. 1998, *Nature*, 392, 895
- Condon, J.J. 1992, *ARAA*, 30, 575
- Cowie, L., & Barger, A. 1999, *astro-ph*. 9907043
- Downes, D. et al. 1999, *A&A*, submitted
- Eales, S. et al. 1999, *ApJ*, 515, 518
- Guilloteau, S., Omont, A., McMahon, R.G., Cox, P., & Petitjean, P. 1997, *A&A*, 328, L1
- Güsten, R. et al. 1993, *ApJ*, 402, 537
- Holland, W. et al. 1999, *MNRAS*, 303, 659
- Kreysa, E. et al. 1999, *SPIE*, 3357, 319
- Madau, P. et al. 1996, *MNRAS*, 283, 1388
- Ohta, K. et al. 1996, *Nature*, 382, 426
- Omont, A. et al. 1996a, *A&A*, 315, 1
- Richards, E. 1999, *ApJ*, 513, 9
- Saunders, R.S. et al. 1990, *MNRAS*, 242, 318
- Smail, I., Ivison, R., Blain, A., Kneib, J.P., & Owen, F. 1999, *astro-ph* 9906196
- Smail, I. et al. 1999, *MNRAS*, in press, *astro-ph* 9905246
- Solomon, P.M., Radford, S.J.E., & Downes, D. 1992, *Nature*, 356, 318
- Downes, D. & Solomon, P. 1998, *ApJ*, 507, 615
- Steidel, C., Adelberger, K., Giavalisco, M., Dickinson, M., & Pettinin, M. 1999, *ApJ*, 519, 1
- Tan, J.C., Silk, J., & Blanford, C. 1999, *ApJ*, in press
- Yun, M.S., Carilli, C.L., Kawabe, R., Tutui, Y., Kohno, K. & Ohta, K. 1999, *ApJ*, submitted